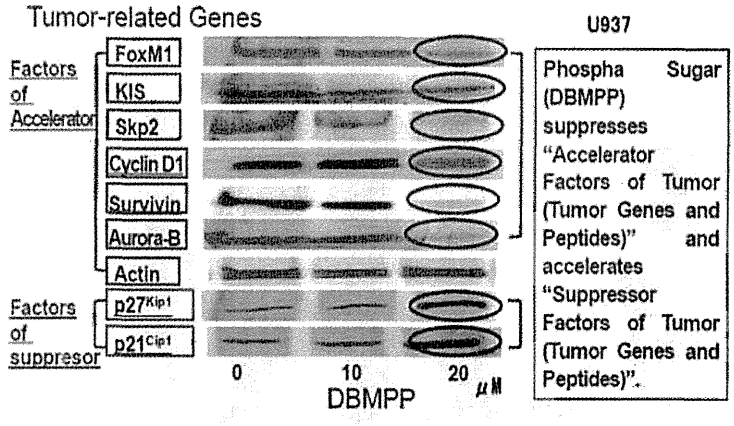

Figure 3 Western blot analysis by DBMPP against U937 cell lines.

to be quite efficient antitumor agents against many kinds of leukemia cell lines and to cure effectively tumor patients suffered from different types of leukemia cell lines.

EXPERIMENTAL

Instruments

TLC (Silica gel: Wako Chromato sheet and/or Merk Kieselgel 60; Eluent : $CHCl_3$: MeOH = 20 : 1, in R*f* value); melting point apparatus (Gallenkamp, in °C) and thermal analysis instrument (Shimazu DTG-60A50AH, TGA and DSC, in °C); HPLC (GL Science: GL-7410 HPLC Pump and GL-7450 UV Detector); MS (MALDI-TOF-MS: GL Science, Voyager-DE Porimerix; Matrix: α-Cyano-4-hydroxycinnamic acid, in *m/z*); IR

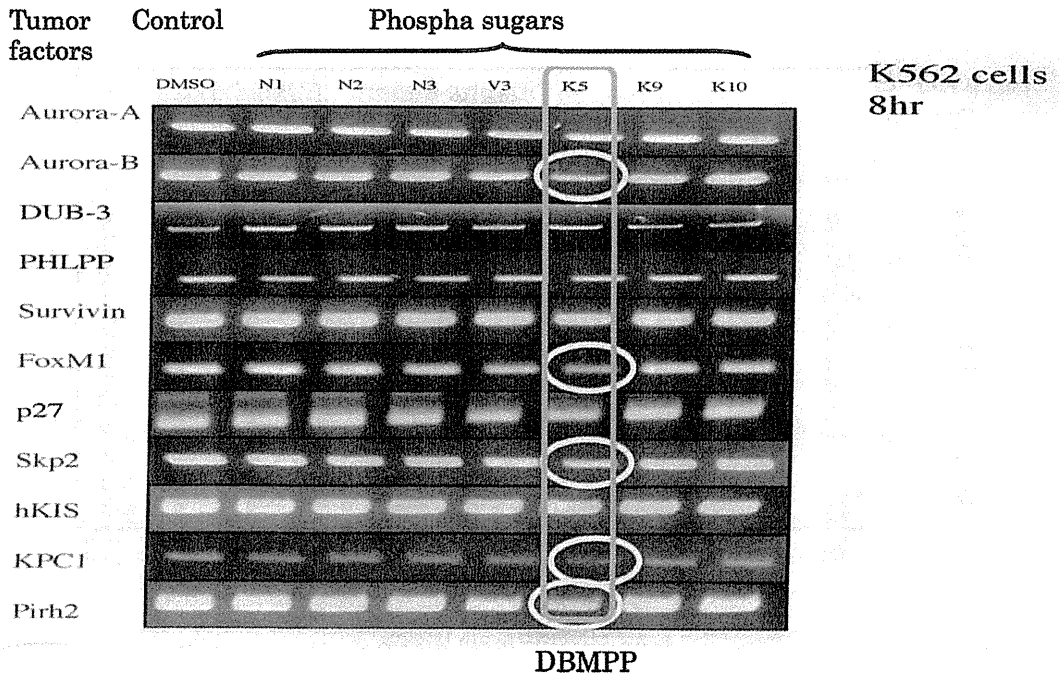

Figure 4 Western blot analysis by DBMPP against K562 cell lines. (Color figure available online).

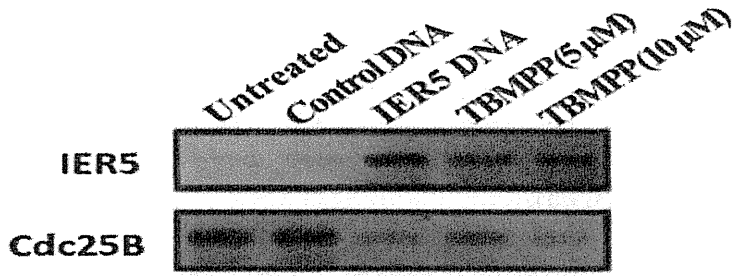

Figure 5 Western blot analysis; Acceleration of IER5 expression and suppression of Cdc25B expression by TBMPP.

(JASCO FT/IR 410 (KBr), in cm^{-1}); ^{1}H-NMR (JEOL JNM-AL300 (300 MHz); Solvent: $CDCl_3$, in δ (ppm) from TMS) were used to record and collect the data for analyzing the products.

Materials

3-Methyl-1-phenyl-2-phospholene 1-oxide (**1**),[15] was prepared and used as the starting material.

Synthesis of 4-bromo-3-methyl-1-phenyl-2-phospholene 1-oxide (2)

3-Methyl-1-phenyl-2-phospholene 1-oxide (**1**: 0.96 g, 5.0 mmol; 1.0 eq.) was dissolved in CCl_4 (5 mL), and to the solution NBS (1.33 g, 1.5 eq.) was added and stirred to make clear solution at 70 °C. To the solution was then added AIBN (0.12 g, 0.75 mmol; 0.15 eq.) and the solution of the reaction mixture was refluxed for 1 day. The reaction mixture was treated with saturated aqueous solution of sodium hydrogensulfite, and then the solution was washed with saturated sodium hydrogencarbonate solution, brine, and water followed by drying over anhydrous Na_2SO_4, which was followed by removal of the solvent afforded crude product. Silica gel column chromatograpy of the product with the mixed eluent of chloroform and methanol (20 : 1) afforded product **2** (0.88 g, 3.3 mmol) in a yield of 65%; Molecular equation: $C_{11}H_{12}BrOP$; M.W.: 271.01; TLC: $R_f = 0.42$ ($CHCl_3$:MeOH = 20 : 1); MS (*m/z*), 271.5(MH^+, 100), 273.5(MH^+, isptope, 90); ^{1}H-NMR ($CDCl_3$, 300 MHz), $\delta = 2.23$ (s, 3H, CH_3), 2.70–2.89 (m, 1H, C5), 2.96–3.15 (m, 1H, C5), 5.14–5.20 (m, 1H, C4), 6.17 (t, $J = 20.1$ Hz, 1H, C2), 7.48–7.65(m, 3H, *o,p*-Ph), 7.80–7.87(m, 2H, *m*-Ph).

Synthesis of 2,3-dibromo-3-methyl-1-phenylphospholane 1-oxide (DBMPP (3))

3-Methyl-1-phenyl-2-phospholene 1-oxide (**1**: 0.21 g, 1.1 mmol; 1.0 eq.) was dissolved in $CHCl_3$ (5 mL), and to the solution Cu(II)Br_2 (0.12 g, 0.53 mmol; 0.49 eq.) was added $CHCl_3$ (10 mL) solution of bromine (0.5 mL; 2.7 g, 17 mmol; 16 eq.) dropwisely and stirred for 1 h at room temperature. The reaction mixture was treated with saturated sodium hydrogensulfite solution and was extracted with $CHCl_3$. The $CHCl_3$ extract was washed with saturated sodium hydrogencarbonate, brine, and water, and then dried over anhydrous Na_2SO_4. Evaporation of the solvent from the solution of the product followed by silica gel column chromatography with the mixed eluent of chloroform and methanol (20

: 1) afforded 2,3-dibromo-3-methyl-1-phenylphospholane 1-oxide (**3**; 0.35 g, 0.99 mmol) in 90% yield as a colorless crystal; Molecular equation: $C_{11}H_{13}Br_2OP$; M.W.: 352; TLC: $R_f = 0.23$ ($CHCl_3$:MeOH = 20 : 1); MS (*m/z*), 351.5 (MH^+, 60), 353.5 (MH^+, isptope peak, 100), 355.5 (MH^+, isptope peak, 40); ^{1}H-NMR ($CDCl_3$, 300 MHz), $\delta = 2.17$ (s, 3H, C3-CH_3), 2.44–2.58 (m, 2H, C5), 2.60–2.83 (m, 2H, C4), 4.67 (dd, $J = 1.5$ Hz, $J = 7.2$ Hz, 1H, C2), 7.32–7.56 (m, 5H, Ph).

Synthesis of 2,3,4-tribromo-3-methyl-1-phenylphospholane 1-oxide (TBMPP (4))

Similarly, the reaction of 4-bromo-3-methyl-1-phenyl-2-phospholene 1-oxide (**2**: 0.16 g, 6.0 mmol; 1.0 eq.) with bromine (1.2 mL; 6.6 g, 41 mmol; 6.8 eq.) in CCl_4 under reflux temperature for 24 h and work-up procedure afforded TBMPP (1.7 g, 4.0 mmol) in 69% yield; Molecular equation: $C_{11}H_{12}Br_3OP$; M.W.: 431; TLC: $R_f = 0.62$ ($CHCl_3$: MeOH = 20 : 1); Mp: 142–144 °C; MS (*m/z*): 429.0 (MH^+, 45), 431.1 (MH^+, isptope, 100), 433.1 (MH^+, isptope, 95), 435.1 (MH^+, isptope, 30); ^{1}H-NMR ($CDCl_3$, 300 MHz), $\delta = 2.14$ (s, 3H, C3-CH_3), 2.73–2.90 (m, 1H, C5), 3.04–3.14 (m, 1H C5), 4.26 (d, $J =$ 1.8 Hz,1H, 4C), 4.68–4.86 (m, 1H, C2), 7.52–7.79 (m, 5H, Ph).

Synthesis of 2-bromo-3-hydroxy-3-methyl-1-phenylphospholane 1-oxide (5)

The reaction of 3-methyl-1-phenyl-2-phospholene 1-oxide (**1**: 0.24 g, 1.3 mmol; 1.0 eq.) with bromine (0.5 mL; 2.7 g, 17 mmol; 13 eq.) in the mixed solvent of $CHCl_3$ (2 mL) and water (8 mL (340 eq.) of diluted sodium hydroxide aqueous solution) under stirring for 3 d at room temperature was progressed. The reaction mixture was treated with saturated sodium hydrogensulfite solution and the product was extracted with $CHCl_3$. The extract was washed with saturated sodium hydrogencarbonate solution, brine, and water, and then the solution of the product was dried over anhydrous Na_2SO_4. Evaporation of the solvent followed by silica gel column chromatography with the mixed eluent of chloroform and methanol (20 : 1) afforded product **5** (0.20 g, 0.69 mmol) in 55% yield; Molecular equation $C_{11}H_{14}BrO_2P$; M.W.: 289; TLC: $R_f = 0.45$ ($CHCl_3$: MeOH = 20 : 1); MS (*m/z*): 289.5 (MH^+), 291.5 (MH^+, isptope); ^{1}H-NMR ($CDCl_3$, 300 MHz): $\delta = 1.69$ (s, 3H, C3-CH_3), 2.01–2.51 (m, 2H, C4, C5), 4.32 (m, 1H, C2), 7.48–7.71 (m, 5H, Ph).

Synthesis of 2-bromo-3-(2-hydroxyethoxy)-3-methyl-1-phenylphospholane 1-oxide (6)

The $CHCl_3$ (2 mL) solution of the mixture of 3-methyl-1-phenyl-2-phospholene 1-oxide (**1**: 0.050 g, 0.26 mmol; 1.0 eq.), ethylene glycol (3 mL, 3.3 g, 53 mmol; 200 eq.), and bromine (0.3 mL; 1.6 g, 10 mmol; 39 eq.) was stirred for 2 d at room temperature. The work-up procedure of the reaction mixture by treating with saturated sodium hydrogensulfite and washing with sodium hydrogencarbonate, brine, and water followed by drying over anhydrous Na_2SO_4 and removal of the solvent, and chromatography on silica gel (eluent: $CHCl_3$: MeOH = 20; 1) afforded product **6** (0.077 g, 0.23 mmol) in a yield of 88%; Molecular equation: $C_{13}H_{18}BrO_3P$; M.W.: 333; TLC: $R_f = 0.15$ ($CHCl_3$: MeOH = 20 : 1);

MS (*m/z*): 333.1 (MH^+, 100), 335.1 (MH^+, isptope, 85); ^{1}H-NMR ($CDCl_3$, 300 MHz), δ = 1.57 (s, 3H, C3-CH_3), 2.10–2.31 (m, 2H, C5), 2.40–2.44 (m, 2H, C4), 3.63–3.65 (m, 2H, -CH_2OH), 3.82–3.85 (m, 2H, -OCH_2-), 4.19 (s, 1H, -OH), 7.50–7.82 (m, 5H, Ph)

Synthesis of 2-bromo-3-(2-(2-hydroxyethoxy)-ethoxy)-3-methyl-1-phenylphospholane 1-oxide (7)

Similarly, the reaction of 3-methyl-1-phenyl-2-phospholene 1-oxide (**1**: 0.050 g, 0.26 mmol; 1.0 eq.) with bromine (0.5 mL; 1.6 g, 10 mmol; 38 eq.) in diethylene glycole (3 mL; 3.3 g, 31 mmol; 120 eq.) for 2 d at room temperature under stirring and the work-up procedure followed by silica gel column chromatography (eluent: $CHCl_3$: MeOH = 20 : 1) afforded product **7** (0.055 g, 0.15 mmol) in 58% yield; Molecular equation $C_{15}H_{22}BrO_4P$; M.W.: 377; TLC: R_f = 0.15 ($CHCl_3$: MeOH = 20 : 1); MS (*m/z*): 377.3 (MH^+, 100), 379.3 (MH^+, isptope, 90); ^{1}H-NMR ($CDCl_3$, 300 MHz), δ = 1.53 (s, 3H, C3-CH_3), 2.07–2.13 (m, 2H, C5), 2.34–2.53 (m, 2H, C4), 3.84 (s, 1H, OH), 3.59–3.84 (m, 8H, -CH_2CH_2-), 4.15–4.17 (m, 1H, C2), 7.46–7.77 (m, 5H, Ph)

Synthesis of 2-Imidazolyl-3-methyl-1-phenyl-2-phospholane 1-oxide (8)

To an acetonitril (3 mL) solution of 4-bromo-3-methyl-1-phenyl-2-phospholene 1-oxide (**2**: 0.050 g, 0.18 mmol; 1.0 eq.) was added imidazole (0.062 g, 0.91 mmol; 5.1 eq.) and the mixture was stirred for 24 h at 60°C. The reaction mixture was worked-up by addition of $CHCl_3$ followed by washing with saturated sodium hydrogencarbonate solution, brine, and water, and then dried over anhydrous Na_2SO_4 followed by removal of the solvent to afford crude product **8**, whose chromatography on silica gel with an eluent of mixed solvent ($CHCl_3$: MeOH = 20 : 1) afforded product **8** (0.042 g, 0.16 mmol) in a yield of 89%; Molecular equation: $C_{14}H_{15}N_2OP$; M.W.: 258; TLC: R_f = 0.2 ($CHCl_3$: MeOH = 20 : 1); MS (*m/z*): 259.5 (MH^+, 100); ^{1}H-NMR ($CDCl_3$, 300 MHz), δ = 1.88 (s, 3H, C3-CH_3), 2.36–2.49 (m, 1H, C5), (2.85–2.95 (m, 1H, C5), 5.16(s, 1H, C2), 6.31 (d, J = 21.6 Hz, im-C4-H), 7.13 (d, J = 20.9 Hz, im-C5-H), 7.52–7.72 (m, 5H, Ph), 7.63 (s, 1H, im-C2-H)

Evaluations and Analyses

MTT In Vitro Evaluation for Phospha Sugars Against Leukemic Cells[13]

Antitumor activities of phospha sugars **2–8** prepared were evaluated by MTT method against K562 (human chronic myelogenous leukemia) and U937 (human acute myelogenous leukemia) cell lines as well as HL60, NB4, YRK2, NOMO-1, CEM, MOLT4, SUP-B15, MEG-01, and SHG3 cell lines. Cells were seeded in 96-well flat-bottomed microplates at a density of 5×10^4 per well and incubated with various concentrations of phospha sugar derivatives for antitumor activity assay or without any phospha sugars for control experiments, for 48 h at 37°C, and then 10 μL solution of 3-(4,5-dimethylthiazol-2-yl)-2,5-diphenyltetrazolium bromide (MTT) (Sigma) was added to each well at the final concentration of 1.0 μg/mL/well. After incubation for 24 h or 48 h at 37°C, absorbance was measured at a wavelength of 560 nm by using a microplate reader for the *in vitro* evaluation.

Cell Cycle Analyses[13]

Propidium iodide (PI) (Sigma) staining was used to analyze cellular DNA content. Cells treated with Imatinib mesylate (Glivec, Gleevec) (1 μM) or phospha sugars DBMPP or TBMPP were cultured at 37°C in 2 mL of complete medium containing 1×10^6 cells. After incubation for 24 h or 48 h, the cells were washed twice with cold PBS, fixed with 70% ethanol overnight before treatment with 100 μg/mL RNase A, and then stained with 50 μg/mL of PI. For apoptosis analysis, the relative DNA content per cell was measured by flow cytometry using an Epics Elite flow cytometer (Coulter Immunotech). The percentage of cells in the apoptotic sub-G1 phase, as well as G1, S, and G2/M phases, was calculated using the ModFit program (Becton Dickinson).

Western Blot Analyses[13,14]

For Phospha Sugar Treated Leukemia Cells. Leukemia cells treated with phospha sugars (DBMPP or TBMPP) were harvested, and then washed with cold PBS, and resuspended in lysis buffer containing 0.5% Nonidet P-40, 50 mM Tris-HCl (pH 8.0), 0.1 mM EDTA, 150 mM NaCl, 1 mM sodium orthovanadate, and 1 mM dithiothreitol supplemented with one Complete Mini protease inhibitor tablet (Boehringer Mannheim GmBH) per 20 mL lysis buffer immediately before use. The proteins were separated by sodium dodecyl sulfate-polyacrylamide gel electrophoresis (SDS-PAGE) and transferred to polyvinylidene difluoride membranes (Millipore). The membranes were then blocked with 0.5% milk in PBS for 1 h at room temperature. After being washed with Tris-buffered saline Tween (TBS-T), the membranes were incubated for 1 h at room temperature with horseradish peroxidase-conjugated goat anti-mouse IgG or anti-rabbit IgG (Amersham Biosciences Inc.) for 1 h and exposed to X-ray film at room temperature. The signal was detected by chemiluminescence using an ECL detection kit (Amersham Bioscience Inc.). The following commercially available antibodies and dilutions were used for Western blot analysis: rabbit polyclonal anti-FoxM1 antibody (MPP2 K-19, 1:500) (Santa Cruz Biotechnology, Inc.), rabbit polyclonal anti-$p27^{Kip1}$ antibody (1:1000) (Santa Cruz Biotechnology, Inc.), mouse monoclonal anti-$p21^{Cip1}$ antibody (1:1000) (Santa Cruz Biotechnology, Inc.), rabbit polyclonal anti-Cdc25B2 antibody (1:500) (Santa Cruz Biotechnology, Inc.), mouse monoclonal anti-Cyclin D1 antibody (1:500) (Santa Cruz Biotechnology, Inc.), mouse monoclonal anti-Cyclin A antibody (1:500) (Santa Cruz Biotechnology, Inc.), rabbit polyclonal anti-KIS antibody (1:500) (ABGENT, Inc.), rabbit polyclonal anti-Aurora-B antibody (1:500) (ABGENT, Inc.), mouse monoclonal anti-bcl-2 antibody (BD Biosciences Pharmingen), mouse monoclonal anti-caspase-9 antibody (BD Biosciences Pharmingen), mouse monoclonal anticaspase-3 (CPP32) antibody (BD Biosciences Pharmingen), and mouse monoclonal anti-PARP antibody (BD Biosciences Pharmingen). To ensure equal protein volume loading, similar experiments were performed by using a mouse monoclonal antiactin antibody (C-4; ICN Biomedicals, Inc., Aurora, OH) as an internal control.

For Transfected Cells. Cells transfected with scrambled shRNA or with IER5 shRNA-#1 or -#2 were harvested. After 3 d, Western blot analysis was performed using the following antibodies: goat polyclonal anti-IER5 (Abcam), rabbit polyclonal anti-Cdc25B (Santa Cruz), anti-CHK1 (Santa Cruz), anti-WEE1 (Santa Cruz), anti-Aurora-B (Santa Cruz), mouse monoclonal anti-Cyclin B1 (Santa Cruz), and anti-Survivin (Santa Cruz). To ensure equal protein volume loading, similar experiments were performed by using a mouse monoclonal antiactin antibody (C-4; ICN Biomedicals, Inc., Aurora, OH) as an internal control.

REFERENCES

1. (a) M. Shan; G. A. O'Doherty. *Org. Lett.*, **2008,** 10, 3381-3384. (b) M. Sollogoub; P. Sinay. "*Organic Chemisry of Sugars*," D. E. Levy and P. Fugedi (Ed.), (CRC Press, Taylor & Francis, New York, NY, USA, **2006**), Chap. 8, pp. 349-381.
2. M. A. Alam; A. Kumar; Y. D. Vankar. *Eur. J. Org. Chem.*, **2008,** 29, 4972-4980.
3. B. Joseph; P. Rollin. *Phosphorus Sulfur Silicon Relat. Elem.*, **1993,** 74, 467-468.
4. M. Yamashita. "*Top. Heterocyclic Chem., Bioactive Heterocycles II*" Ed. by S. Eguchi, (Springer, Berlin, Germany, **2007**), **8**, pp. 173-222.
5. R. L. Whistler; C. C. Wang. *J. Org. Chem.*, **1968,** 33, 4455-4458.
6. (a) S. Inouye; T. Tsuruoka; T. Ito; T. Niida. *Tetrahedron*, **1968,** 24, 2125-2144. (b) M. Shan; G. A. O'Doherty. *Org. Lett.* **2008,** 10, 3381-3384. (c) M. A. Alam; A. Kumar; Y. D. Vankar. *Eur. J. Org. Chem.* **2008,** 29, 4972-4980. (d) B. G. Davis; M. A, Maughan; T. M. Chapman; R. Villard; S. Courtney. *Org. Lett.* **2002,** 4, 103-106. (e) M. Chmielewski; R. L. Whistler. *J. Org. Chem.* **1975,** 40, 639-643. (f) P. Wang; L. A. Agrofoglio; M. G. Newton; C. K. Chu. *J. Org. Chem.* **1999,** 64, 4173-4178.
7. (a) G. Legler; E. Julich. *Carbohydr. Res.* **1984,** 128, 61-72. (b) J. Braanalt; I. Kvarnstroem; G. Niklasson; S. C. T. Svensson; B. Classon; B. Samuelsson. *J. Org. Chem.* 59, 1783-1788 (**1994**).
8. (a) E. M. Dangerfield; C. H. Plunkett; B. L. Stocker; M. S. M. Timmer. *Molecules*, **2009,** 14, 5298-5307. (b) S. Martinez-Montero; S. Fernandez; Y. S. Sanghvi; J. Chattopadhyaya; M. Ganesan; N. G. Ramesh; V. Gotor; M. Ferrero. *J. Org. Chem.*, **2012,** 77, 4671-4678.
9. (a) B. Joseph; P. Rollin. *J. Carbohydr. Chem.*, **1993,** 12, 719-29. (b) V. Blot; J.-F. Brier; M. Davoust; S. Miniere; V. Reboul; P. Metzner. *Phosphorus, Sulfur Silicon Relat. Elem.*, **2005,** 180, 1171-1182.
10. (a) T. Hanaya; K. Sugiyama; Y. Fujii; A Akamatsu; H. Yamamoto. *Heterocycles*, **1994,** 55, 1301-1309. (b) T. Hanaya; S. Kawase; H. Yamamoto. *Heterocycles*, **2005,** 66, 251-261. (c) M. Yamashita; Y. Nakatsukasa; M. Yoshikane; H. Yoshida; T. Ogata; S. Inokawa. *Carbohydr. Res.* **1977,** 59, 12-14. (d) H. Yamamoto; T. Hanaya; H. Kawamoto; S. Inokawa; M. Yamashita; M. A. Armour; T. T. Nakashima. *J. Org. Chem.* **1985,** 50, 3516-3521.
11. (a) M. Yamashita; Y. Kato; K. Suzuki; T. Oshikawa. *Heterocycl. Commun.* **1998,** 4, 411-414. (b) V. Krishna Reddy; B. Haritha; T. Oshikawa; M. Yamashita. *Tetrahedron Lett.* **2004,** 45, 2851-2854. (c) M. Yamada; K. Asai; J. Yamashita; T. Suyama; T. Niimi; K. Maddali; M. Fujie; S. Nakamura; M. Kimura; Y. Tanaka; M. Toda; M. Yamashita. *Heterocycl. Commun.* **2010,** 16, 173-180.
12. (a) M. Yamaoka; M. Yamashita; M. Yamada; M. Fujie; K. Kiyofuji; N. Ozaki; K. Asai; T. Niimi; T. Suyama; J. Yamashita; A. Sawada; R. Makita; M. Sugiyama; M. Toda; S. Nakamura; K. Ohnishi. *Pure Appl. Chem.*, **2012,** 84, 37-48. (b) K. Tsunekawa; M. Yamashita; M. Fujie; T. Niimi; T. Suyama; K. Asai, S. Ito; J. Yamashita; M. Yamada; N. Ozaki; S. Nakamura. *Phosphorus, Sulfur Silicon Relat. Elem.*, **2011,** 186, 936-944. (c) J. Yamashita; T. Suyama; K. Asai; M. Yamada; T. Niimi; M. Fujie; S. Nakamura; K. Ohnishi; M. Yamashita. *Heterocyclic Commun.*, **2010,** 16, 89-97. (d) M. Yamada; M. Yamashita; T. Suyama; J. Yamashita; K. Asai; T. Niimi; N. Ozaki; M. Fujie; K. Maddali; S. Nakamura; K. Ohnishi. *Bioorg. Med. Chem. Lett.*, **2010,** 20, 5943-5946.
13. S. Nakamura; M. Yamashita; D. Yokota; I. Hirano; T. Ono; M. Fujie; K. Shibata; T. Niimi; T. Suyama; K. Maddali; K. Asai; J. Yamashita; Y. Iguchi; K. Ohnishi. *Invest. New Drugs*, **2010,** 28, 381-391.
14. S. Nakamura; Y. Nagata; L. Tan, T. Takemura; K. Shibata; M. Fujie; S. Fujisawa; Y. Tanaka; M. Toda; R. Makita; K. Tsunekawa; M. Yamada; M. Yamaoka; J. Yamashita; K. Ohnishi;, M. Yamashita. *PLoS One*, **2011,** 6, e28011.
15. M. Yamashita; R. P. Mallikarjuna; Y. Kato; V. Krishna Reddy; K. Suzuki; T. Oshikawa, *Carbohydr. Res.*, **2001,** 336, 257-270.

Molecular and Cellular Biology

Regulatory Nexus of Synthesis and Degradation Deciphers Cellular Nrf2 Expression Levels

Takafumi Suzuki, Tatsuhiro Shibata, Kai Takaya, Kouya Shiraishi, Takashi Kohno, Hideo Kunitoh, Koji Tsuta, Koh Furuta, Koichi Goto, Fumie Hosoda, Hiromi Sakamoto, Hozumi Motohashi and Masayuki Yamamoto

Mol. Cell. Biol. 2013, 33(12):2402. DOI: 10.1128/MCB.00065-13.
Published Ahead of Print 9 April 2013.

MCB
Journals.ASM.org

Regulatory Nexus of Synthesis and Degradation Deciphers Cellular Nrf2 Expression Levels

Takafumi Suzuki,[a] Tatsuhiro Shibata,[b] Kai Takaya,[a] Kouya Shiraishi,[c] Takashi Kohno,[c] Hideo Kunitoh,[d] Koji Tsuta,[e] Koh Furuta,[e] Koichi Goto,[f] Fumie Hosoda,[b] Hiromi Sakamoto,[g] Hozumi Motohashi,[h] Masayuki Yamamoto[a,i]

Department of Medical Biochemistry[a] and Center for Radioisotope Sciences,[h] Tohoku University Graduate School of Medicine, and Tohoku Medical-Megabank Organization,[i] Sendai, Japan; Divisions of Cancer Genomics,[b] Genome Biology,[c] and Genetics,[g] National Cancer Center Research Institute, and Divisions of Pathology and Clinical Laboratories, National Cancer Center Hospital,[e] Tokyo, Japan; Department of Respiratory Medicine, Mitsui Memorial Hospital, Tokyo, Japan[d]; Division of Thoracic Oncology, National Cancer Center Hospital East, Kashiwa City, Chiba, Japan[f]

Transcription factor Nrf2 (NF-E2-related factor 2) is essential for oxidative and electrophilic stress responses. While it has been well characterized that Nrf2 activity is tightly regulated at the protein level through proteasomal degradation via Keap1 (Kelch-like ECH-associated protein 1)-mediated ubiquitination, not much attention has been paid to the supply side of Nrf2, especially regulation of *Nrf2* gene transcription. Here we report that manipulation of *Nrf2* transcription is effective in changing the final Nrf2 protein level and activity of cellular defense against oxidative stress even in the presence of Keap1 and under efficient Nrf2 degradation, determined using genetically engineered mouse models. In excellent agreement with this finding, we found that minor A/A homozygotes of a single nucleotide polymorphism (SNP) in the human *NRF2* upstream promoter region (rs6721961) exhibited significantly diminished *NRF2* gene expression and, consequently, an increased risk of lung cancer, especially those who had ever smoked. Our results support the notion that in addition to control over proteasomal degradation and derepression from degradation/repression, the transcriptional level of the *Nrf2* gene acts as another important regulatory point to define cellular Nrf2 levels. These results thus verify the critical importance of human SNPs that influence the levels of transcription of the *NRF2* gene for future personalized medicine.

The *Nrf2* (NF-E2-related factor 2; or *Nfe2l2*) gene encodes a basic leucine zipper-type transcription factor that belongs to the CNC (cap'n'collar) family (1). Nrf2 displays its transactivation activity through dimerization with one of the small Maf (sMaf) proteins, and the Nrf2-sMaf heterodimer recognizes a specific DNA sequence known as the antioxidant (ARE)/electrophile response element (EpRE) (2, 3). Downstream target genes of Nrf2 include enzymes that act in detoxifying and antioxidative stress responses, enzymes related to glutathione synthesis, and transporters, which together constitute a network to facilitate the cellular adaptation to oxidative and xenobiotic stresses (4, 43). Studies with the *Nrf2* gene knockout ($Nrf2^{-/-}$) mouse clearly demonstrate that Nrf2 deficiency attenuates the response to oxidative and electrophilic stresses (5, 6), resulting in high-level susceptibility to a variety of toxic chemicals and carcinogens (7–9). Similarly, Nrf2-deficient mice are prone to the initiation of carcinogenesis, demonstrating that Nrf2 contributes to cancer chemoprevention (10–12). Conversely, large numbers of cancer cells express high levels of Nrf2, and this fact indicates that cancer cells hijack and exploit Nrf2 activity for their malignant growth (13–15).

One of the important characteristics of Nrf2 is the inducible nature of its function in response to oxidative and electrophilic stresses (16). Under homeostatic and stress-free conditions, cellular Nrf2 abundance is maintained at a very low level, as the ubiquitin E3 ligase complex composed of Keap1 (Kelch-like ECH-associated protein 1) and cullin 3 specifically promotes ubiquitination and proteasomal degradation of Nrf2 (16, 44). Notably, Keap1 acts as a sensor for electrophilic and oxidative stresses by using reactive cysteine residues within the protein (17). Exposure to electrophiles or reactive oxygen species hampers Keap1 activity, reducing Nrf2 ubiquitination and leading to the stabilization and nuclear translocation/accumulation of Nrf2 (17). Subsequently, the expression of a battery of Nrf2 target genes is induced for cytoprotection against these insults. Thus, cellular Nrf2 activity is induced by a derepression mechanism utilizing the proteasomal protein degradation machinery (4).

Multiple lines of evidence support the mechanism of Nrf2 derepression from proteasomal degradation, which accounts for the inducible expression of Nrf2 target genes. On the contrary, changes in the supply side of Nrf2 seem to be less significant under these stress conditions than the derepression/accumulation mechanism of the Nrf2 protein (18). Thus, not much attention has been paid to the contribution of transcriptional regulation of the *Nrf2* gene to the accumulation of Nrf2 protein and inducible expression of its target genes. However, several lines of evidence suggest the importance of the transcriptional regulation of the *Nrf2* gene. For instance, the *Nrf2* mRNA level was found to increase approximately 2-fold 6 h after treatment of an electrophile in murine keratinocytes (19).

A promoter single nucleotide polymorphism (SNP) of the mouse *Nrf2* gene was found to be tightly linked to the sensitivity/

Received 16 January 2013 **Returned for modification** 31 January 2013
Accepted 1 April 2013
Published ahead of print 9 April 2013
Address correspondence to Masayuki Yamamoto, masiyamamoto@med.tohoku.ac.jp.
Takafumi Suzuki and Tatsuhiro Shibata contributed equally to this article.
Supplemental material for this article may be found at http://dx.doi.org/10.1128/MCB.00065-13.

doi:10.1128/MCB.00065-13

resistance of various inbred mouse lines to the toxicity of high concentrations (95%) of oxygen (8). Similarly, a variant of the *NRF2* gene in the upstream promoter region (rs6721961) (20) is associated with susceptibility to acute lung injury in humans (21). This human SNP is located in the middle of the ARE motif and weakens the affinity of NRF2 binding to the ARE. This regulatory SNP (rSNP) appears to disrupt the positive-feedback regulation of *NRF2* expression by NRF2 itself (21). Other consequences of this *NRF2* rSNP have also been reported, including the risk of venous thromboembolism (22), reduced vital capacity (23), and an impaired forearm vasodilator response (24).

However, it remains to be determined how significantly the *Nrf2* transcript level affects Nrf2 definitive activity *in vivo*. This is the most critical issue for the future use of this and related *NRF2* SNPs in risk assessment and personalized medicine. Therefore, to address this critical issue, we have exploited genetically engineered mouse models. Our present results unequivocally demonstrate the importance of the level of the Nrf2 supply in both the presence and absence of Keap1-mediated protein degradation regulation. In addition, in order to clarify how significantly the reduction of the *NRF2* mRNA level is linked to the pathogenesis of human diseases, we explored whether the *NRF2* rSNP rs6721961 contributes to the increased risk of non-small-cell lung carcinomas. We compared the incidence of each genotype of the *NRF2* rSNP in a lung cancer population and a control population. We also measured the endogenous expression of *NRF2* in immortalized lymphocytes. We found that the rSNP genotype indeed affects the *NRF2* mRNA level in peripheral lymphocytes and also brings about an increased risk of non-small-cell lung cancers. These results strongly argue that transcription of the *NRF2* gene is an important regulatory point for cellular NRF2 activity.

MATERIALS AND METHODS

Mice. *Nrf2*$^{-/-}$ and Keap1 gene knockout (*Keap1*$^{-/-}$) mice were produced and characterized as described previously (6, 25). Transgene construct *KRD*-Nrf2 was generated by subcloning the Flag-hemagglutinin (HA)-tagged mouse Nrf2 cDNA into the vector harboring a 5.7-kb *Keap1* gene regulatory domain (*KRD*) (26). Transgenic mice were generated as described previously (26). Four independent lines were established for *KRD*-Nrf2. All compound mutant mice examined in this study were from a mixed genetic background, with contributions from 129Sv/J, C57BL/6J, and ICR strains. For hematoxylin-eosin (H&E) staining, the esophagi of P10 pups or adult mice were fixed in 3.7% formalin and embedded in paraffin.

Cell culture. Peritoneal macrophages were isolated as described previously (5). Whole-cell extracts were prepared in a lysis buffer (26) and subjected to immunoblot analysis using anti-Nrf2 (27), anti-Flag (Sigma-Aldrich), anti-HA (Roche), and anti-α-tubulin (Sigma-Aldrich) antibodies. Cell viability after 1-chloro-2,4-dinitrobenzene (CDNB) treatment was determined using a Cell Counting Kit-8 (Dojin Laboratories) according to the manufacturer's protocol. Diethyl maleate (DEM) and CDNB were purchased from Wako Pure Chemicals. Menadione and benzyl isothiocyanate (BITC) were purchased from Sigma-Aldrich.

Real-time PCR. Total RNA was prepared from forestomachs or macrophages using an Isogen RNA extraction kit (Nippon Gene) or from immortalized lymphocytes using an RNeasy kit (Qiagen). The cDNAs were synthesized from the total RNA using SuperScript III reverse transcriptase (Invitrogen by Life Technology). Real-time quantitative PCR was performed using an ABI 7300 (Applied Biosystems by Life Technology) or LightCycler 480 (Roche) system. Primer and probe sequences are available upon request.

Study participants. All lung cancer cases and controls were Japanese. These cases received treatments at the National Cancer Center Hospitals (NCCH), Japan, from 2000 to 2008. All surgically collected lung cancer specimens were pathologically examined by at least two board-certified pathologists in the NCCH. Histological diagnosis is based on the WHO classification of lung tumors (28). The controls were volunteers enrolled at the NCCH and at Keio University, located in Tokyo, Japan, with the following inclusion criteria: they could not have lung or other cancers or a history of cancer. All cases and controls, all of whom provided informed consent, were consecutively included in this study without any exclusion criteria. This study was approved by the institutional review boards of the National Cancer Center. Smoking habit was expressed by the number of pack-years, which was defined as the number of cigarette packs smoked daily multiplied by the number of years of smoking. Those who had never smoked (never smokers) were defined as individuals for whom the number of pack-years was 0. Those who had ever smoked (ever smokers) were defined as individuals for whom the number of pack-years was >0 and included both former and current smokers.

SNP analysis. Genomic DNA was extracted from whole blood from lung cancer cases and controls enrolled in the NCCH. Genomic DNA was extracted from Epstein-Barr virus-transformed B lymphocytes derived from whole blood collected from volunteers enrolled at Keio University. Genomic DNA was extracted using a blood maxikit or a QIAamp DNA minikit (Qiagen). The genotypes of NRF2 rSNP rs6721961 (referred to here as NRF2 rSNP-617) were determined by TaqMan SNP genotyping assays (Applied Biosystems by Life Technology).

Detection of somatic *EGFR* and *KRAS* mutations in lung tumors. Tumor samples were obtained at the time of surgery, rapidly frozen in liquid nitrogen, and stored at −80°C. Genomic DNA from the tissues was extracted using a QIAamp DNA minikit (Qiagen). Somatic mutations in the *EGFR* and *KRAS* genes were examined by high-resolution melting analysis (HRMA) as previously described (29).

Statistical analysis. Odds ratios (ORs) and 95% confidence intervals (CIs) for lung adenocarcinoma (ADC) risk were calculated after adjusting for gender, age (≤49, 50 to 59, 60 to 69, and ≥70 years), and smoking (never smoker versus ever smoker) by unconditional logistic regression analysis. These analyses were performed using JMP (version 8.0) software (SAS Institute Inc., Cary, NC).

RESULTS

Reflection of *Nrf2* gene dosage on cellular Nrf2 activity. To clarify how significantly reduction of *Nrf2* synthesis affects Nrf2 activity *in vivo*, we decided to exploit genetically engineered mouse models and examine whether transcriptional regulation of the *Nrf2* gene makes a substantial contribution to Nrf2 activity. Because Keap1 represses Nrf2 activity by accelerating the proteasomal degradation of the Nrf2 protein, a *Keap1*-null background provides an ideal model to analyze the gene dosage effect of *Nrf2*. Importantly, in this model system we can ignore the influence of Nrf2 degradation provoked by the Keap1-based ubiquitination of Nrf2. Indeed, *Keap1* gene knockout results in the constitutive accumulation of Nrf2, and the *Keap1*-null background is lethal in pups due to severe hyperkeratosis of the upper digestive tract (25). These phenotypes of the *Keap1*-null mice can be restored by simultaneous deletion of the *Nrf2* gene, indicating that the *Keap1*-null phenotype is attributable to the hyperactivation of Nrf2 (25).

When we deleted the *Nrf2* gene heterozygously in Keap1-deficient (i.e., *Keap1*$^{-/-}$::*Nrf2*$^{+/-}$) mice, we found a partial rescue of the severe phenotype of *Keap1*-null mice in the compound mutant mice. In contrast to the *Keap1*-null (*Keap1*$^{-/-}$::*Nrf2*$^{+/+}$) mice, the *Keap1*$^{-/-}$::*Nrf2*$^{+/-}$ mice survived to adulthood, as was the case for *Keap1*-null mice with the complete knockout of Nrf2 (*Keap1*$^{-/-}$::*Nrf2*$^{-/-}$). This indicates that deletion of a single allele

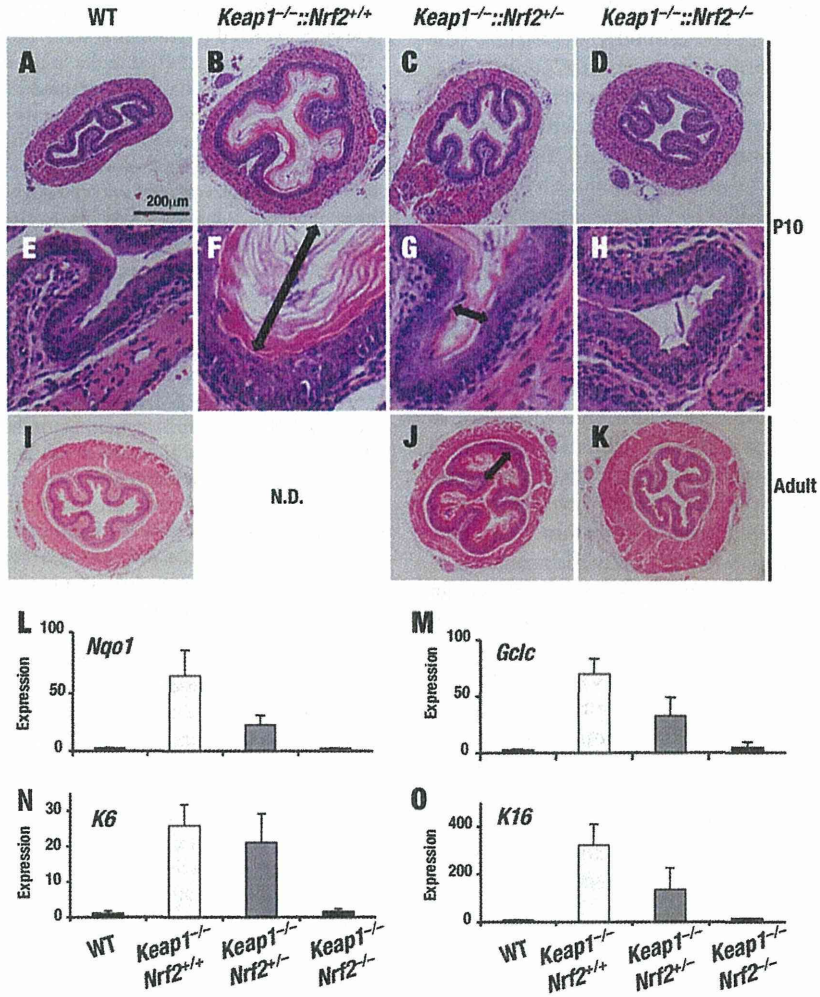

FIG 1 Heterozygous deletion of the *Nrf2* gene alleviates lethal phenotypes of Keap1-deficient mice. (A to K) H&E staining of transverse sections of the esophagus from P10 (A to H) and adult (I to K) mice. Lower (A to D) and higher (E to H) magnifications of the pictures are shown. Arrows indicate the thickened cornified layer. (L to O) Relative expression levels of the *Nqo1*, *Gclc*, *K6*, and *K16* genes compared with the level of 18S rRNA gene expression in the forestomachs of P10 mice. Data are the means ± SDs ($n = 3$). WT, wild type; N.D., no data.

of the *Nrf2* gene is sufficient to rescue the lethality caused by the Keap1 deficiency. We found that the average body weight of the *Keap1*$^{-/-}$::*Nrf2*$^{+/-}$ mice was less than that of the *Keap1*$^{-/-}$::*Nrf2*$^{-/-}$ mice in both males and females (see Fig. S1A and B in the supplemental material). Consistent with our previous observations (25), the *Keap1*$^{-/-}$::*Nrf2*$^{+/+}$ mice showed severe thickening of the cornified layers in the esophagus at 10 days after birth (Fig. 1B and F). On the contrary, the *Keap1*$^{-/-}$::*Nrf2*$^{+/-}$ mice showed clear improvement in the cornification and thickening (Fig. 1C and G). In adult *Keap1*$^{-/-}$::*Nrf2*$^{+/-}$ mouse esophagi, however, the thickening of the cornified layer became apparent (Fig. 1J). These results thus demonstrate that while the Nrf2 level synthesized from a single allele contributes to the esophageal phenotype to a certain extent in the *Keap1* knockout background (*Keap1*$^{-/-}$::*Nrf2*$^{+/-}$), it gives rise to a phenotype much milder than that resulting from the Nrf2 level synthesized from two alleles in the *Nrf2* wild-type background (*Keap1*$^{-/-}$::*Nrf2*$^{+/+}$).

Consistent with the esophageal phenotypes, the levels of expression of Nrf2 target genes, such as *Nqo1* [NAD(P)H:quinone oxidoreductase 1] and *Gclc* (glutamate-cysteine ligase catalytic subunit), and keratin-related genes, including *K6* (keratin 6) and *K16* (keratin 16), were lower in the forestomachs of *Keap1*$^{-/-}$::*Nrf2*$^{+/-}$ mice than in those of *Keap1*$^{-/-}$::*Nrf2*$^{+/+}$ mice but were higher than those in the forestomachs of *Keap1*$^{-/-}$::*Nrf2*$^{-/-}$ mice (Fig. 1L to O). Specifically, the levels of expression in the forestomachs of *Keap1*$^{-/-}$::*Nrf2*$^{+/-}$ mice were approximately half of the levels in *Keap1*$^{-/-}$::*Nrf2*$^{+/+}$ mice, indicating the presence of haploinsufficiency in *Nrf2* gene expression. These results thus indicate that the *Nrf2* gene dosage has an impact on Nrf2 activity *in vivo*.

Nrf2 synthesis is a critical determinant of cytoprotection capacity. Our next question was whether the Nrf2 transcription level affects the cellular capacity of cytoprotection even in the presence of Keap1-mediated Nrf2 degradation. To this end, we adopted thioglycolate-elicited mouse peritoneal macrophages as an experimental system, as this peritoneal macrophage system is well established as a system for testing the roles played by Nrf2 in the stress response (5). We first confirmed that in Nrf2 heterozygous